

HUMAN BODY EFFECTS ON INKJET-PRINTED FLEXIBLE RF INTERCONNECTIONS

Shahed Alam, Hannu P. Sillanpää, and Riku M. Mäkinen*

Department of Electronics, Tampere University of Technology,
P. O. Box 692, Tampere FI-33101, Finland

Abstract—The effect of human body on inkjet-printed flexible single-layer transmission lines in immediate proximity of body is investigated by simulations and measurements up to 9 GHz. A multiline extraction method is used to obtain effective material parameters allowing detailed analysis of body effects. Already at 1 mm distance from the body, the line properties converge toward the free-space values. However, at smaller distances and in direct contact with the body, often required in biosensor applications, there is a significant change in characteristic impedance and increase in losses. The results of the paper can be used to evaluate the body effects at different frequencies and at different small distances from the body.

1. INTRODUCTION

The effect of human body on antenna performance in wearable and body-worn applications has been extensively studied [1–3]. The close proximity of human body with a high dielectric constant and loss are known to have a detrimental effect on antenna input impedance and efficiency. Other research areas on wearable technology concentrate on wireless body-area networks (BAN) [3, 4], wearable systems carried in clothing [5], and realization of fabric antennas [6] or stretchable interconnections [7, 8]. Research on medical applications concentrate on the biomedical data with less emphasis on the body-worn wireless link [9]. The medical devices may also be external off-body applicators [10]. Human body effects are considered in [11], where models for signal propagation inside tissue are presented for biomedical implant applications.

However, the effect of human body on the performance of radio-frequency (RF) interconnections and electronics near human body

Received 13 November 2012, Accepted 12 December 2012, Scheduled 12 December 2012

* Corresponding author: Riku M. Mäkinen (riku.makinen@tut.fi).

has received surprisingly little attention. The body affects the characteristic impedance of the transmission lines causing mismatch, changes the electrical length, and significantly increases losses, thus potentially deteriorating the operation of an RF circuit. Information on the distance when the body begins to affect the operation of a circuit and how significant the effect is need to be considered in RF design. In addition, the suitability of commercial design tools for body-worn RF design needs to be established. This is critical in particular for biosensors placed in direct contact with or few tenths of a millimeter from the body.

In this work, we investigate the effect of human body on single-layer high-frequency interconnections. The thin flexible lightweight interconnections suitable for body-worn applications are realized using printable electronics technology [12,13]. The co-planar waveguide (CPW) is used as a test structure. The analysis is carried out using commercial simulation software package AWR Microwave Office [14] by introducing lossy body material in the substrate definition stack. The material properties for muscle available in [15] are used in the simulations. The simulation results are validated by on-substrate measurements up to 9 GHz using vector network analyzer (VNA) with a probe station. In the measurements, a cut of fresh beef is used to approximate muscle.

In order to gain further insight into the body effects on high-frequency interconnections, wide-band extraction methods can be used to obtain attenuation constant, characteristic impedance, and effective material parameters for the lines [16–18]. In this work, an improved multilayer extraction method [19–21] based on the multilayer thru-reflect-line (TRL) calibration method [22] is applied to both simulation and measurement data. This allows detailed and accurate wide-band analysis of dielectric loading and additional loss due to the body.

The remainder of the paper is organized as follows. The inkjet-printed test structures, simulation model, and measurement setup with and without lossy substrate are presented in Section 2. The multilayer extraction method is briefly reviewed in Section 3. Finally, the simulated and measured results are presented and guidelines are provided in Section 4. Section 5 concludes the paper.

2. ANALYSIS OF BODY EFFECTS ON RF INTERCONNECTIONS

2.1. Test Structures

The test set that consist of varying length of coplanar waveguide (CPW) transmission lines are displayed in Fig. 1. The single-layer

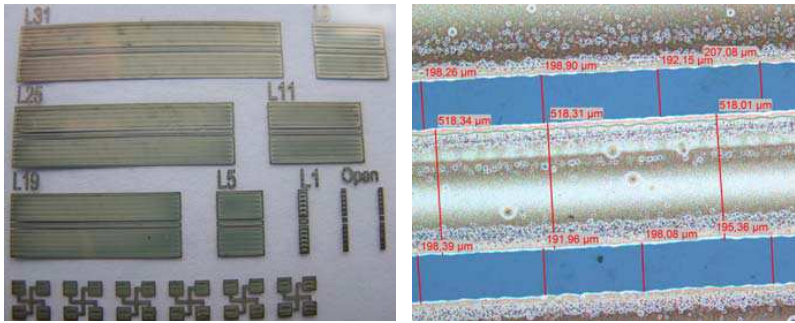


Figure 1. Inkjet-printed CPW characterization test set and a microscope image of a line detail.

CPW is selected due to its suitability for the printing process to realize interconnections and its easy interfacing with the measurement probes. The CPW traces are made of silver nano-particle ink and the traces are printed on 50- μm polyethylene naphthalate (PEN) substrate. The Greek crosses that are visible in the test set in Fig. 1 are used to measure the sheet resistance R_S [23]. The average value of the measured R_S was 90 m Ω corresponding to 1.1E07 S/m conductivity for 1- μm conductor thickness. Fig. 1 also shows the microscopic top view of the CPW with dimensions of conductor gap and centre conductor width at different positions of the CPW. The average values of the CPW gap and centre conductor are 190 μm and 520 μm , respectively, and these values are also adopted in simulations.

2.2. Simulation Model

The simulations are carried out using AWR Microwave Office simulation software by using the AXIEM electromagnetic (EM) field solver. The simulation model consists of four layers. The first layer consists of 3 traces of CPW with centre conductor width set to 520 μm , the width of the two ground planes is assigned to 3 mm and the gap between the center line and ground plane is fixed to 190 μm . The measured dc sheet resistance was used as a starting point for the determination of high-frequency conductivity for the simulation model. Good agreement with high-frequency simulations and measurements was obtained with $R_S = 105 \text{ m}\Omega$ which was subsequently adopted in simulations. In AWR, this was defined by setting the conductor thickness to 1 μm and conductivity to 9.5E06 S/m. In the second layer, the substrate properties for the 50- μm PEN film substrate are introduced by assigning the loss tangent to 0.01 and the relative permittivity to 3.35. Third layer of the model characterizes the air

gap and it is placed between the body and the CPW in the air gap simulations but in simulations in contact with the body the air layer is excluded. The bottom layer characterizes the muscle and assigned the frequency-dependent relative permittivity and loss tangent shown in Fig. 2 [15]. For free space simulation only the first two layers are considered and the bottom layer is set to open boundary.

2.3. Measurement Setup

Line-reflect-match (LRM) calibration was used to calibrate the Agilent E8358A PNA using the impedance standard substrate (ISS) 106-682 and the Cascades Microtech WinCal software. A microwave probe station with 800- μm ground-signal-ground (GSG) probes was used for measurements. The measurements were performed on two different platforms. For the in air measurements, a 2-mm low-loss microwave foam with permittivity close to 1 has been used and for on body measurements, fresh beef of 5 mm thickness is used as platform as shown in Fig. 3. The fresh beef was wrapped with a film of plastic and in order to protect the probe station. The chosen plastic film was very thin to minimize the effect on the measurements. In order to emulate the bends that can take place on interconnections in body-worn RF circuits, pieces of microwave foam of different dimensions were used. Different lengths of CPW were measured on the microwave foam with varying bends. Measurements were repeated several times to ensure the accuracy.

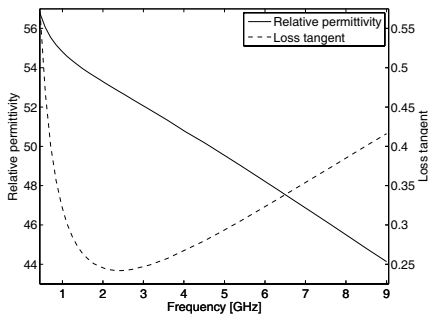


Figure 2. Electrical material properties for muscle tissue [15].

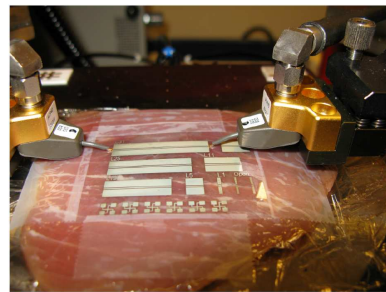


Figure 3. VNA measurement setup with probe station for CPW lines in direct contact with lossy substrate. Fresh beef is used to emulate human body tissue (muscle).

3. MULTILINE EXTRACTION METHOD

Transmission line-measurement based characterization methods are suitable for characterization of both conductors and dielectrics using VNA measurements. Single line-pair based characterization methods can be used for printable electronics characterization [16–18]. However, the relatively large manufacturing tolerances associated with inkjet-printed transmission lines and the half-wave resonances decrease the accuracy of the methods using a single line pair. These problems can be avoided by using the multiline material characterization method [19, 20]. The improved accuracy is achieved through redundant measurements. Typically, the redundant standards are transmission lines of different lengths, which additionally improves the applicable bandwidth.

The transmission lines are modeled with three cascaded networks; an intrinsic line segment is embedded between error boxes R_A and R_B as shown in Fig. 4. The error boxes model the transition from the probe-head to the transmission line and other possible discontinuities and pad parasitics at the line ends. The characterization begins with a first-tier calibration that provides known reference impedance and sets the reference plane to the probe-tips. The multiline material characterization method consists of two main phases: firstly the multiline TRL calibration [22] is used to solve the propagation constant of the lines and the error boxes at both ends of the lines. The multiline TRL method weights the measurements from multiple line pairs at each frequency so that optimally weighted propagation constant and error boxes are achieved.

The second step is to fit an equivalent circuit to the error-box network parameters which enables to solve the characteristic impedance of the transmission lines. The π equivalent circuit is used which has been shown to give accurate results for printed transmission lines [20]. The propagation constant and characteristic impedance can then be used to calculate the distributed transmission line parameters R , L , G , and C and further to solve the effective permittivity and the loss tangent of the dielectric $\tan \delta_{eff}$.

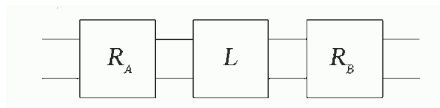


Figure 4. A transmission line consisting of error boxes R_A , R_B and an intrinsic line length L .

4. RESULTS AND DISCUSSION

In this section, the characteristics of high frequency interconnections are analyzed as the distance between the muscle and CPW transmission line is varied. The measurement and simulation data are presented, and validity of simulation results is established by comparison to measurements. Simulations are performed using AXIEM solver integrated in the AWR Microwave Office simulation software. Measurements are carried out up to 9 GHz using Agilent E8358A PNA and a microwave probe station with 800- μm GSG probes. The LRM calibration referenced to $50\ \Omega$ is used in the measurements. The test sets consist of CPW lines of different lengths, i.e., 5 mm, 9 mm, 11 mm, 13 mm, 19 mm, 25 mm, 31 mm and TRL calibration THRU (1 mm) and REFLECT standards. The presented results are obtained by applying a second-tier multilayer TRL calibration to the first-tier LRM data and subsequently extracting the results.

The multilayer extraction method removes impedance mismatch and half-wave resonances, thus providing wide-band data without any unwanted irregularities in the result that would increase complication in the analysis. The multilayer method also allows separation of conductor and dielectric properties. The data presented includes attenuation constant α , resistance per unit length of the line R , effective loss tangent $\tan \delta_{eff}$, effective permittivity $\epsilon_{r,eff}$, and characteristic impedance Z_0 . The attenuation constant depicts the total loss whereas R and $\tan \delta_{eff}$ reveal the contribution of the conductor and dielectric loss. Finally, Z_0 and $\epsilon_{r,eff}$ provide insight in the impedance level and phase velocity of the lines.

First, the simulation results are validated by measurements by investigating the attenuation constant α . The attenuation constant for different values for air gap is shown in Fig. 5. The measurements are carried out in free space by using a low-loss microwave foam as a substrate and on fresh beef sample emulating muscle tissue. In simulations, the material parameters given in Section 2 were used. The values of α obtained from on air simulation converges fittingly with the free space measurements. However, the on body simulated curve is approximately 0.7 dB above the measured curve due to the thin plastic film and the air gap which inevitably exists in the measurements between the PEN substrate and fresh beef. The fact that the measurement curve is located between the in contact and 10 μm air gap curve illustrates the sensitivity of the attenuation constant to air gap when placed very close to body. The good agreement between simulations and measurements validate the simulation approach.

The effect of air gap on attenuation constant can then be evaluated

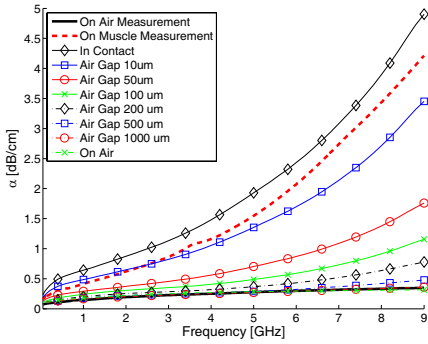


Figure 5. Extracted attenuation constant α from simulations and measurements.

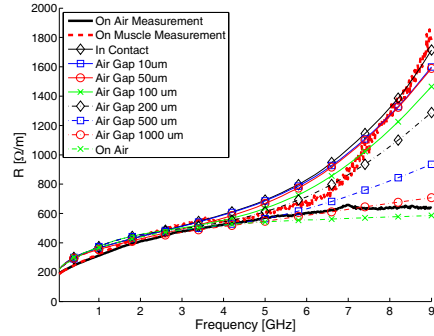


Figure 6. Extracted resistance per unit length R from simulations and measurements.

by simulations. At lower frequencies up to 3.5 GHz, α is less than 0.5 dB/cm for air gaps down to 50 μm . Even in direct contact, α is of the order of 1 dB/cm. At higher frequencies, a radical reduction in loss is observed as the air gap is increased from 10 μm to 50 μm . For an air gap larger than 0.5 mm, α is below 0.5 dB/cm throughout the frequency range. For 1 mm air gap, the simulated curve approximately merges with the free-space measurement.

The measured and simulated values of resistance per unit length R are presented in Fig. 6. Measured results are presented for the lines in direct contact with the body and in free space. Below 5 GHz, the resistance R is independent of the air gap. This is the expected result as the lossy conductors remain the same in all simulations and measurements. However, above 5 GHz R increases when the air gap is less than 0.5 mm. This occurs for both measured and simulated results indicating the phenomenon is real. To understand the sharp rise, simulations with PEC interconnections (i.e., $R = 0$) where performed and the results showed similar increase in R above 5 GHz. Therefore, it can be stated that the increase observed in the conductor losses is due to the muscle which begins to act as lossy ground plane at higher frequencies. For the air gap approaching 0.5 mm to 1.0 mm, the simulated results converge toward the free-space measurement throughout the frequency band.

The measured and simulated effective loss tangent $\tan \delta_{eff}$ is presented in Fig. 7. Again when the air gap approaches 1.0 mm, $\tan \delta_{eff}$ converges toward the free-space measurement indicating no effect due to muscle. However, as the air gap is reduced, $\tan \delta_{eff}$ increases dramatically. The measurement and simulation results for

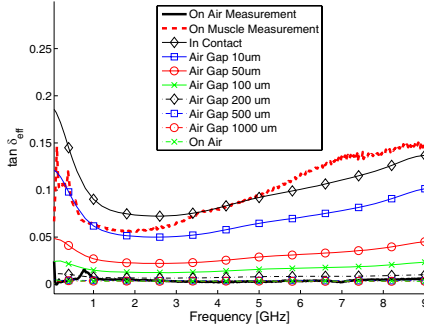


Figure 7. Extracted effective loss tangent $\tan \delta_{eff}$ from simulations and measurements.

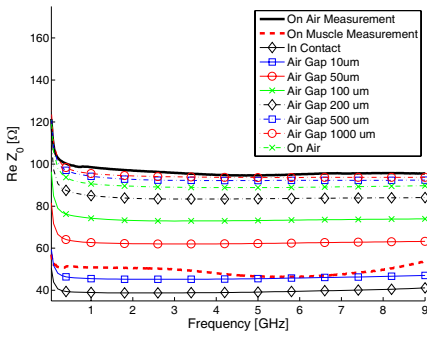


Figure 8. Extracted (real part) characteristic impedance $\Re(Z_0)$ from simulations and measurements.

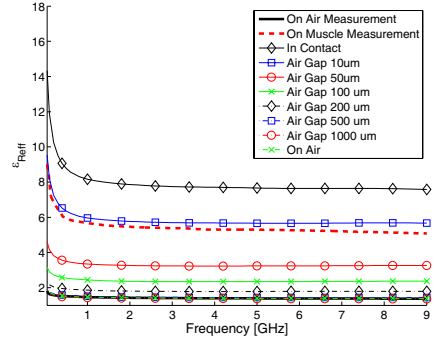


Figure 9. Extracted effective permittivity $\epsilon_{r,eff}$ from simulations and measurements.

direct contact with muscle agree well, indicating the fresh beef used in the measurements corresponds to the muscle tissue properties given in Section 2. The small variations observed in the measurement and simulation is due to the small yet inevitable air gap always present in the measurements as well as the difference between the muscle properties used in simulations and measurements.

Finally, the real part of characteristic impedance and effective relative permittivity are shown in Fig. 8 and Fig. 9, respectively. The simulations agree well with measurements, however, in direct contact with muscle there is difference in both impedance and $\epsilon_{r,eff}$. For example, it can be observed from the Fig. 8 that as the interconnection is placed over the muscle the impedance value at 9 GHz is 53 Ω in

measurements and 41Ω in simulations, the difference is due to the small air gap present in the measurements. This is indicated by the fact that the simulation with a $10 \mu\text{m}$ air gap agrees well with the measurement in direct contact with the muscle. However, in immediate proximity of the body, the impedance in Fig. 8 changes from the free-space value of approximately 95Ω to 50Ω due to dielectric loading of the body. Similarly, $\epsilon_{r,eff}$ in Fig. 9 increases from approximately 1.3 to 6. These significant changes in impedance level and electrical length (i.e., phase shift over a length of an interconnection) may significantly affect the operation of RF circuits. It is important to consider this in the design for RF electronics in immediate proximity of the human body. With a 0.5 mm to 1.0 mm air gap, the results again converge toward the free-space values.

In addition to the effect of human body on RF interconnections, also the effect of bending typical for body-worn and wearable applications was studied in VNA measurements up to 9 GHz . Microwave foam was used as a substrate. However, regardless of very small bending radii tested, virtually no change in line properties were observed. It is therefore concluded that in contrast to antennas, bending does not have a significant effect on RF interconnections.

The results presented in Fig. 5 through Fig. 9 indicate that the body has little effect on RF interconnections when the distance to the body is of the order of 0.5 mm to 1.0 mm or larger. The body effects can therefore be neglected in RF design (of course, antennas excluded) for most wearable applications where electronics is integrated in clothing typically at a safe, well over 1 mm distance from the body. However, below 0.5 mm distance from the body, the line properties and in particular the loss were significantly affected by the presence of human body. This is of importance in applications such as biosensors where the sensor must be located in immediate proximity or in direct contact with the body. The effect increases dramatically with increasing frequency. At 2.4 GHz , the loss is approximately 1 dB/cm for a CPW in contact with the body. For a miniaturized design, even this may be acceptable level of loss. However, at 9 GHz the loss increases to 4 dB/cm which may deteriorate the performance of the RF circuit. However, even a small air gap between the film substrate and body helps to reduce the loss.

In this work, a commercial RF circuit simulator with EM solver was used to analyze inkjet-printed interconnections on human body. Despite the very unusual electrical properties of human body to be used in RF simulator, the measurements successfully validated the simulation approach for body-worn RF design. In addition to body-worn RF design in general, this is relevant for example for the design

of a balun or matching circuit between an integrated RF radio chip and a body-worn antenna for a wireless sensor. Finally, the recently introduced multiline extraction method was successfully used to obtain detailed and accurate wide-band information from both simulations and measurements.

5. CONCLUSION

The effect of human body on RF interconnections was investigated by simulations and measurements up to 9 GHz. The multiline extraction technique was successfully used to provide further insight into the results. For distances above 0.5 mm from the body, virtually no effect was observed. However, in immediate proximity with the body, a significant change in line properties was observed. The increase in loss and changes in characteristic impedance and phase velocity that may significantly affect the performance of an RF circuit and need to be considered. Finally, by comparison with measurement data, the work also validated the use of a commercial RF simulator for body-worn RF design. The results are important for RF design in applications requiring immediate contact with the body such as biosensors.

ACKNOWLEDGMENT

This work is funded by the Academy of Finland.

REFERENCES

1. Kellomäki, T., "Effects of the human body on single-layer wearable antennas," Ph.D. Thesis, Tampere University of Technology, Tampere, 2012.
2. Sankaralingam, S. and B. Gupta, "Development of textile antennas for body wearable applications and investigations on their performance under bent conditions," *Progress In Electromagnetics Research B*, Vol. 22, 53–71, 2010.
3. Hall, P. S. and Y. Hao, *Antennas and Propagation for Body-centric Wireless Communications*, Artech House, London, 2006.
4. Tseng, H.-W., S.-T. Sheu, and Y.-Y. Shih, "Rotational listening strategy for IEEE 802.15.4 wireless body networks," *IEEE Sensors Journal*, Vol. 11, No. 9, 1841–1855, 2011.
5. Chedid, M., I. Belov, and P. Leisner, "Electromagnetic coupling to a wearable application based on coaxial cable architecture," *Progress In Electromagnetics Research*, Vol. 56, 109–128, 2006.

6. Osman, M. A. R., M. K. Abd Rahim, N. A. Samsuri, H. A. M. Salim, and M. F. Ali, "Embroided fully textile wearable antenna for medical monitoring applications," *Progress In Electromagnetics Research*, Vol. 117, 321–337, 2011.
7. Axisa, F., F. Bossuyt, T. Vervust, and J. Vanfleteren, "Laser based fast prototyping methodology of producing stretchable and conformable electronic systems," *Proc. Electronics System-integration Technol. Conf.*, 1387–1390, London, Sep. 2008.
8. Loher, T., M. Seckel, and A. Ostmann, "Stretchable electronics manufacturing and application," *Proc. Electronics System-integration Technol. Conf.*, 1–6, Berlin, Sep. 2010.
9. El-Nasr, M. A., H. A. Shaban, and R. M. Buehrer, "Key design parameters and sensor-fusion for low-power wearable UWB-based motion tracking and gait analysis systems," *Progress In Electromagnetics Research Letters*, Vol. 29, 115–126, 2012.
10. Gupta, R. C. and S. P. Singh, "Development and analysis of a microwave direct contact water-loaded box-horn applicator for therapeutic heating of bio-medium," *Progress In Electromagnetics Research*, Vol. 62, 217–235, 2006.
11. Theilmann, P. T., M. A. Tassoudji, E. H. Teague, D. F. Kimball, and P. M. Asbeck, "Computationally efficient model for UWB signal attenuation due to propagation in tissue for biomedical implants," *Progress In Electromagnetics Research B*, Vol. 38, 1–22, 2012.
12. Mäntysalo, M., V. Pekkanen, K. Kaija, J. Niittynen, S. Koskinen, E. Halonen, P. Mansikkamäki, and O. Hämeenoja, "Capability of inkjet technology in electronics manufacturing," *Proc. 59th Electronic Components and Technology Conf.*, 1330–1336, San Diego, CA, May 2009.
13. Pynttäre, V., R. Mäkinen, V. Palukuru, K. Östman, H. Sillanpää, T. Kanerva, T. Lepistö, J. Hagberg, and H. Jantunen, "Application of wide-band material characterization methods to printable electronics," *IEEE Trans. Electronics Packaging Manufacturing*, Vol. 33, No. 3, 221–227, 2010.
14. AWR Microwave Office, AWR Corporation, Referred Oct. 1, 2012, <http://www.awrcorp.com/>.
15. "Dielectric properties of body tissues," Referred Oct. 1, 2012, Available Online: <http://niremf.ifac.cnr.it/tissprop/>.
16. Carchon, G. and B. Nauwelaers, "Accurate transmission line characterisation on high and low-resistivity substrates," *IEE Proc. Microwaves, Antennas and Propagation*, Vol. 148, No. 5, 285–290, 2001.

17. Mangan, A. M., S. P. Voinigescu, M.-T. Yang, and M. Tazlauanu, "De-embedding transmission line measurements for accurate modeling of IC designs," *IEEE Trans. Electron. Devices*, Vol. 53, No. 2, 235–241, 2006.
18. Sillanpää, H., J. Lilja, R. Mäkinen, K. Östman, V. Palukuru, J. Virtanen, V. Pynttäre, T. Kanerva, J. Hagberg, T. Lepistö, H. Jantunen, and P. Mansikkamäki, "Application of wide-band material parameter extraction techniques to printable electronics characterization," *Proc. 59th Electronic Components and Technology Conf.*, 1342–1348, San Diego, CA, May 2009.
19. Sillanpää, H., A. Rasku, and R. Mäkinen, "A multilayer material parameter extraction method," *Proc. Mediterranean Microwave Symp.*, 314–317, Gzelyurt, Cyprus, Aug. 2010.
20. Rasku, A., H. Sillanpää, I. Hiltunen, and R. Mäkinen, "Multilayer material parameter extraction method performance analysis," *Proc. Asia-Pacific Microwave Conf.*, 1905–1908, Yokohama, Japan, Dec. 2010.
21. Mäkinen, R., A. Rasku, and H. Sillanpää, "Modeling-based printed electronics characterization," *Proc. IEEE Antennas Propagat. Intl. Symp.*, 1–2, Chicago, IL, Jul. 2012.
22. Marks, R. B., "A multilayer method of network analyzer calibration," *IEEE Trans. Microwave Theory Tech.*, Vol. 39, No. 7, 1205–1215, 1991.
23. Enderling, S., C. L. Brown, III, S. Smith, M. H. Dicks, J. T. M. Stevenson, M. Mitkova, M. N. Kozicki, and A. J. Walton, "Sheet resistance measurement of non-standard cleanroom materials using suspended Greek cross test structures," *IEEE T. Semicond. Manuf.*, Vol. 19, No. 1, 2–9, 2006.